Evidence of Dynamical Effects and Critical Field in a Cobalt Spin Crossover Complex

SCHOLARONE™
Manuscripts

Evidence of Dynamical Effects and Critical Field in a Cobalt Spin Crossover Complex

Thilini K.Ekanayaka,[a] Ping Wang,[b] Saeed Yazdani,[c] Jared Paul Phillip,[c] Esha Mishra,[a] Ashley S. Dale,[c] Alpha T. N'Diaye,[d] Christoph Klewe,[d] Padraic Shafer,[d] John Freeland,[e] Robert Streubel,[a,f] James Paris Wampler,[g] Vivien Zapf,[g] Ruihua Cheng,[c]* Michael Shatruk,[b] Peter A. Dowben[a]*

The [Co(SQ)$_2$(4-CN-py)$_2$] complex exhibits dynamical effects over a wide range of temperature. The orbital moment, determined by X-ray magnetic circular dichroism (XMCD) with decreasing applied magnetic field, indicates a nonzero critical field for net alignment of magnetic moments, an effect not seen with the spin moment of [Co(SQ)$_2$(4-CN-py)$_2$].

Finite temperatures can have a profound influence on the on/off ratio for a molecular memory device, with deleterious consequences.[1] For spintronic device applications, it is important to understand the finite temperature effects on the magnetic moments as the devices will have more practical value if there is reliable operation at room temperature and above.

The majority of molecular magnetic systems are characterized by localized magnetic moments that are randomly oriented at zero applied magnetic field, due to weak exchange coupling between molecules. Under an applied magnetic field, the moments orient with fidelity that depends on the field strength. Although the molecular magnetic moments align along the field, the net magnetization typically decreases with increasing temperature and the molar magnetic susceptibility scales inversely proportional with the temperature because the thermal excitations of magnons causes spins to misalign with the magnetic field.[2]

Finite temperature effects obviously occur for molecules where there is a spin state change with temperature. For such spin crossover (SCO) molecules, the magnetic susceptibility deviates from the simple 1/T dependence owing to the conversion from the low spin (LS) to the high spin (HS) state, at which point the susceptibility increases with a degree of abruptness, depending on the cooperativity of SCO.[3–6] At temperatures exceeding the spin state transition temperature, the net measured "collective" magnetic moment in the HS state continues to decrease with temperature.[3–6] So there are other finite temperature effects beyond the change in spin state, but for SCO molecules and indeed other local moment molecular magnets, this has not been investigated in detail, with just a few exceptions.[7]

Spin crossover (SCO) molecules, including those with valence tautomeric transition, have been studied using X-ray absorption spectroscopy (XAS)[8,9] at the transition metal L$_3$-edge to characterize the spin state occupancy[1,7,10-15] by probing the unoccupied states though the electric dipole-allowed excitation of 2p core electrons into the partially filled spin-split 3d orbitals. If the molecule is photoactive, as is the case with many SCO complexes,[7,13,15-21] XAS can perturb the spin state by exciting the molecule from the ground LS state via intersystem crossing to the metastable HS state, which can be trapped at sufficiently low temperatures. This X-ray fluence induced transition to the high spin state is analogous to such LS-to-HS conversions as light-induced excited spin state trapping (LIESST),[11,22-26] soft X-ray-induced excited spin state trapping (SOXIESST)[11,27-28] and hard X-ray-induced excited spin state trapping (HAXIESST).[29] If XAS reliably places the molecule in the high spin state, then X-ray magnetic circular dichroism (XMCD) can be used to probe the temperature dependence of relative spin and orbital moment contributions to the local moment. There are, in fact, a few XMCD studies on SCO molecular films. Bernien et al.[30] performed XMCD to confirm the SOXIESST process for the SCO complex [Fe^{II}(bpz)$_2$phen] (bpz = dihydrobis(pyrazolyl)borate, phen = 1,10-phenanthroline). XMCD has also been employed to establish the influence of the substrate on the spin state occupancy of SCO thin films of [Fe^{II}(phen)$_2$(NCS)$_2$].[31] Apart from

a. Department of Physics and Astronomy, Jorgensen Hall, University of Nebraska, Lincoln, NE 68588-0299, U. S. A.

b. Department of Chemistry and Biochemistry, Florida State University, 95 Chieftan Way, Tallahassee, FL 32306, U. S. A.

c. Department of Physics, Indiana University-Purdue University Indianapolis, Indianapolis, Indiana 46202, U. S. A.

d. Advanced Light Source, Lawrence Berkeley National Laboratory, Berkeley, CA 94720, U. S. A.

e. Argonne National Laboratory, Advanced Photon Source, Bldg. 431/E003, 9700 South Cass Ave., Argonne, IL 60439, U. S. A.

f. Nebraska Center for Materials and Nanoscience, University of Nebraska-Lincoln, Lincoln, NE 68588.

g. National High Magnetic Field Lab, Los Alamos National Laboratory, P.O. Box 1663, Los Alamos, NM 87545, U. S. A.
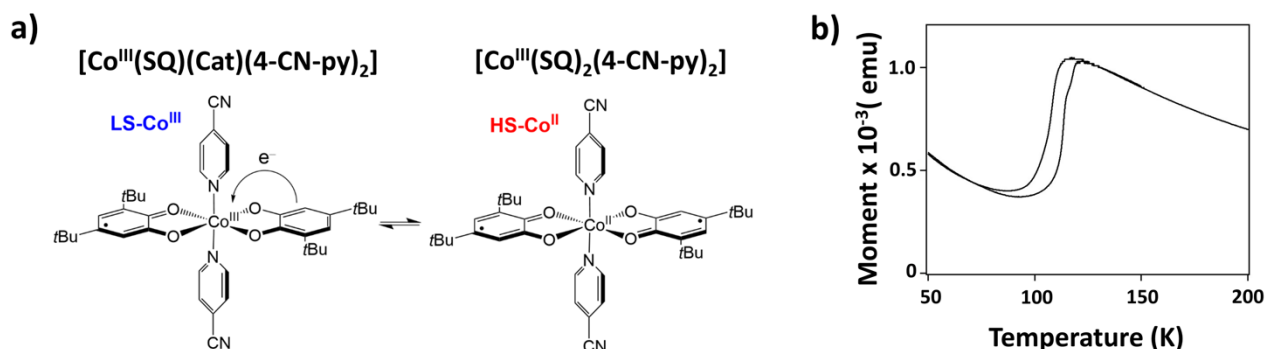
Fig. 1 a) Schematic diagram of $[Co(SQ)(Cat)(4\text{-}CN\text{-}py)_2]$ in LS state and $[Co(SQ)_2(4\text{-}CN\text{-}py)_2]$ in HS state. The arrow indicates the direction of temperature- or radiation-induced ligand-to-metal electron transfer that converts the LS-CoIII center into the HS-CoII center. b) Magnetic susceptibility of $[Co(SQ)(Cat)(4\text{-}CN\text{-}py)_2]/[Co(SQ)_2(4\text{-}CN\text{-}py)_2]$ powder prior to thin film fabrication.

a recent study on the SCO complex $[Fe(bpz)_2(bipy)]$ (bipy = 2,2'-bipyridine),[7] there have been no studies reported to observe the relative spin and orbital moment contributions to the local magnetic moment.

In this study, we report the temperature- and field-dependent XMCD of a cobalt complex that exhibits a valence tautomeric transition[23,24,32,33] from the LS $[Co^{III}(SQ)(Cat)(4\text{-}CN\text{-}py)_2]$ to the HS $[Co^{II}(SQ)_2(4\text{-}CN\text{-}py)_2]$, where Cat = 3,5-di-tert-butylcatecholate, SQ = 3,5-ditert-butylsemiquinonate, and 4-CN-py = 4-cyanopyridine. With the spin transition at the metal center, an electron from the diamagnetic catecholate (Cat) ligand is transferred to the LS-Co(III) center which yields a HS-Co(II) ion and a radical semiquinonate (SQ) ligand.[23,24] This valence tautomeric transition is schematically shown in Figure 1a. The LIESST state induced by photo-conversion from the LS $[Co^{III}(SQ)(Cat)(4\text{-}X\text{-}py)_2]$ to HS $[Co^{II}(SQ)_2(4\text{-}X\text{-}py)_2]$ is long lived below 50 K and, while observed up to 90 K,[23,24] is increasingly short lived for X = CN,[23,24] Br,[24] and NO_2.[24]

The complex $[Co^{II}(SQ)_2(4\text{-}X\text{-}py)_2]$ was synthesized as described previously[23,24,29,33] (see the supplementary for further details). The 100 nm-thick $[Co^{II}(SQ)_2(4\text{-}X\text{-}py)_2]$ thin film onto a highly-oriented pyrolytic graphite (HOPG) substrate as described in the supplementary, where we also provide considerable evidence that $[Co^{II}(SQ)_2(4\text{-}X\text{-}py)_2]$ preserves its molecular structure when deposited as a thin film. HOPG was chosen because this is one of the few substrates that have little influence on the spin state of a SCO molecule.[25,26,30]

Field dependent XMCD spectroscopy was performed at the Advanced Photon Source beamline 4-ID-C at Argonne National Laboratory. The XMCD spectra near the Co $L_{2,3}$-edge were obtained at 200 K and magnetic bias fields (0.5 to 2 T/μ_0). The temperature dependent X-ray absorption and XMCD spectroscopy were carried out at the Advanced Light Source bending magnet beamline 6.3.1 and undulator beamline 4.0.2 at Lawrence Berkeley National Laboratory using a magnetic field of 3.6 T/μ_0 for the XMCD. Both the XAS and XMCD spectra were acquired in the in the total electron yield mode, and for the XMCD results presented here, the applied magnetic field was normal to the plane of the thin film. Since this magnetic field strength is insufficient to align and saturate the magnetic moments, the measured values for the spin and orbital moments will be a small fraction of the actual Co(II) moments.

We also note that the various beamlines employed for this study differ in the ellipticity of the light, resulting in variations in the XMCD spectra, particularly variations in the spin to orbital moment ratios plotted in Figures 3 and 4.

Temperature-dependent X-ray photoemission spectroscopy (XPS) measurements were taken as a function of temperature at photon energy of 1486.6 eV (Al Kα X-ray source) with a SPECS PHOIBOS 150 hemispherical energy analyzer with 20 eV pass energy.[22]
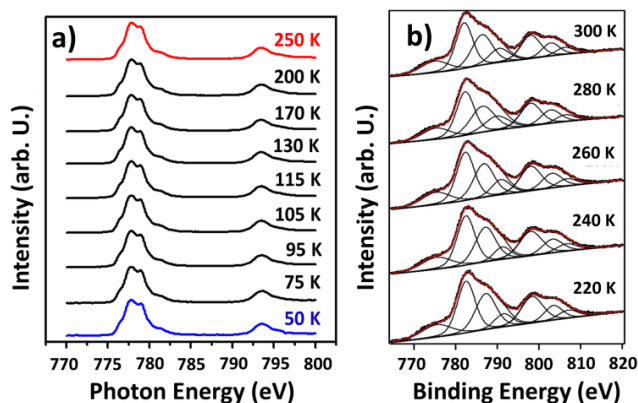

Fig. 2 Temperature dependent XAS (a) and XPS (b) spectra, taken at Co 2p core level, of a $[Co(SQ)_2(4\text{-}CN\text{-}py)_2]$ thin film.

The temperature dependent magnetic susceptibility data of $[Co(SQ)_2(4\text{-}CN\text{-}py)_2]$ reveal a spin state transition temperature of about 110 K and a hysteresis of 5 K (Figure 1b), in agreement with previous observations.[23] In the LS state, the complex exists in the S = 1/2 ground state due to the unpaired electron of the SQ radical. In the HS state, the magnetic susceptibility is due to contributions from the S = 3/2 HS Co(II) ion and two S = 1/2 SQ radicals. In contrast to the magnetic data, the XAS spectra (Figure 2a) show little evidence of a spin state transition. Some small changes are observed between 50 to 250 K, but these changes are almost negligible (see the supplementary for further details). The multiplet fitting of the XPS spectra at 220 K to 300 K are also shown in Figure 2b. The peak shape of the XPS spectrum remains unaffected by temperature, indicating the absence of a redistribution of multiplet intensities known to accompany SCO in transition metal complexes.[18,22,34,35] These observations indicate that the system, exposed to soft X-ray
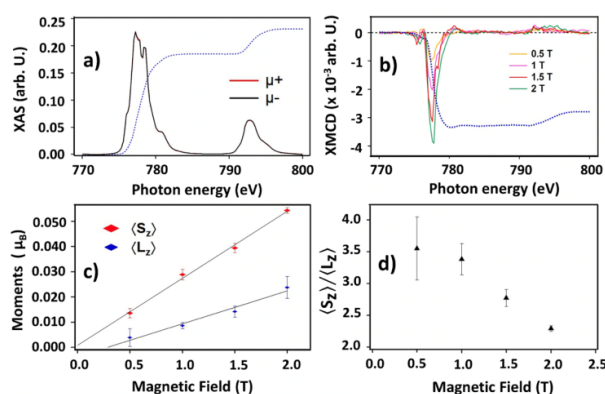
Fig. 3 Field dependent XMCD on [Co(SQ)$_2$(4-CN-py)$_2$] thin films in the HS state on HOPG at 200 K. a) XAS spectra and b) field dependent XMCD signal at Co L-edge. c) Spin and orbital moments with respect to applied magnetic field. d) Spin to orbital moment ratio with respect to magnetic field.

fluence, is mostly in the HS state even at low temperature, which is consistent with the small change in bond lengths reported elsewhere.[33]

Field and temperature dependent XMCD measurements near the Co $2p_{3/2}$ (L$_3$) and $2p_{1/2}$ (L$_2$) edges were performed (Figures 3 and 4) to ascertain the behavior of the spin and orbital magnetic moments. The XMCD intensity increases with the magnetic field (Figure 3b). The orbital and spin moments are calculated from the integrals of both XAS and XMCD spectra (dashed lines in Figures 3a and 3b) defined as,

$$r = \int_{L_3+L_2} (\mu_+ + \mu_-) d\omega, \text{ and } q = \int_{L_3+L_2} (\mu_+ - \mu_-) d\omega, p = \int_{L_3} (\mu_+ - \mu_-) d\omega^{[36]}$$

where $\mu+$ and $\mu-$ are the XAS intensities taken with left and right circular polarization or opposing applied magnetic fields. The orbital and spin moments are shown in Figure 3c with respect to the applied magnetic field strength.

The linear increase with magnetic field indicates that both spin and orbital moments are not saturated at an applied field of 2 T/μ_0. Extrapolation of the spin moment to zero at zero applied magnetic field corroborates a negligible net remanence magnetization indicative of paramagnetic behavior. While both the spin and orbital moment decrease with decreasing magnetic field, the orbital moment has a critical field barrier of 3.4 kOe. This means that a critical field is required for the orbital moments to become evident. As shown in the supplementary materials, choosing different subsets of the available data could reduce the critical field to 1.6 kOe, but not to zero.

Such critical fields stem from barriers caused by the ligand field in the [Co(SQ)$_2$(4-CN-py)$_2$] complex, including anisotropy barriers (see the supplementary for a more detailed discussion). The ratio of the spin to orbital moment, estimated from the XMCD spectra according to <S$_z$>/<L$_z$> = (9p − 6q)/2q,[36] is shown in Figure 3d. Here, p and q are obtained from the integrated XMCD signals at the L$_3$ and L$_2$ edges, respectively, as shown in Figure 3b. The <S$_z$>/<L$_z$> ratio decreases with increasing magnetic field from 3.6 at 0.5 T/μ_0 to 2.2 at 2 T/μ_0, which agrees

well with the expected spin to orbital moment ratio for the HS-Co(II) ion (3.44 to 2.3).[37]

The temperature dependent XMCD of a 100 nm-thick film of [Co(SQ)(Cat)(4-CN-py)$_2$] on a HOPG substrate is shown in Figure 4. The data was recorded in the presence of a magnetic field 3.6 T/μ_0 to increase the signal-to-noise ratio. As seen in Figure 4b, the XMCD signal decreases with increasing temperature. The spin and orbital moments are calculated using the sum rules[35] and integrals of XAS and XMCD spectra (Figures 4a and 4b) and shown in Figure 4c. When increasing the temperature from 150 K to 250 K, the spin moment (Figure 4c) shows a significant decrease consistent with the decline in overall moment above 140 K (Figure 1b). This change can be attributed to thermal magnon excitations which cause a spin moment misalignment even with an applied magnetic field. The resulting projection of spins in the minority spin channel decreases the net spin moment, consistent with the decreasing magnetization with temperature seen in Figure 1b. While the present XMCD results indicate that the spin moment is sensitive to temperature, for another SCO system, [Fe{H$_2$B(pz)$_2$}$_2$(bipy)], the orbital moment, not the spin moment, was found to be sensitive to temperature.[7]

It is evident that, even in the HS state, [Co(SQ)$_2$(4-CN-py)$_2$] exhibits a barrier to orbital moment alignment while the spin moment is clearly temperature dependent. While [Co(SQ)$_2$(4-CN-py)$_2$] is a photoactive material, easily excited from the LS-
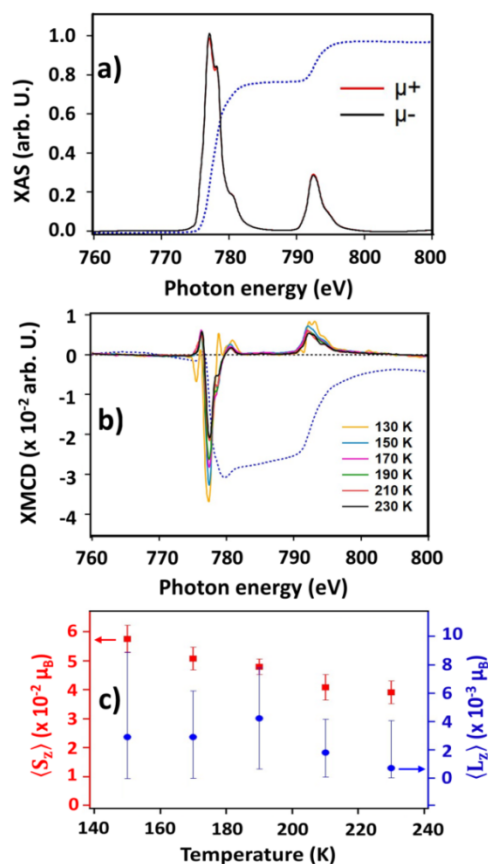

Fig. 4 Temperature dependent XMCD for [Co(SQ)$_2$(4-CN-py)$_2$] thin films on HOPG. a) X-ray absorption spectra and b) temperature dependent XMCD signal at Co L-edge. c) Spin and orbital moments with respect to temperature.

Co^{III} to the HS-Co^{II} state, it should be noted that finite temperature effects are likely to affect all local moment molecular systems.

Conflicts of interest

There are no conflicts to declare.

References

1 G. Hao, R. Cheng, P. A. Dowben, *J. Physics: Condensed Matter* 2020, **32**, 234002.
2 J. S. Miller and M. Drillon, Eds., *Magnetism: molecules to materials*, Wiley-VCH, Weinheim ; New York, 2001.
3 A. Bousseksou, G. Molnár, L. Salmon and W. Nicolazzi, *Chem. Soc. Rev.*, 2011, **40**, 3313.
4 P. Gütlich and H. A. Goodwin, Eds., *Spin crossover in transition metal compounds I-III*, Springer, Berlin ; New York, 2004.
5 P. Gütlich, A. Hauser and H. Spiering, *Angew. Chem. Int. Ed. Engl.*, 1994, **33**, 2024–2054.
6 M. A. Halcrow, Ed., *Spin-crossover materials: properties and applications*, Wiley, Chichester, West Sussex, United Kingdom, 2013.
7 G. Hao, A. T. N'Diaye, T. K. Ekanayaka, A. S. Dale, X. Jiang, E. Mishra, C. Mellinger, S. Yazdani, J. W. Freeland, J. Zhang, R. Cheng, X. Xu and P. A. Dowben, *Magnetochemistry* 2021, in press
8 G. Poneti, M. Mannini, L. Sorace, P. Sainctavit, M.-A. Arrio, E. Otero, J. Criginski Cezar and A. Dei, *Angewandte Chemie International Edition*, 2010, **49**, 1954–1957.
9 H. W. Liang, T. Kroll, D. Nordlund, T.-C. Weng, D. Sokaras, C. G. Pierpont and K. J. Gaffney, *Inorg. Chem.*, 2017, **56**, 737–747.
10 X. Zhang, P. S. Costa, J. Hooper, D. P. Miller, A. T. N'Diaye, S. Beniwal, X. Jiang, Y. Yin, P. Rosa, L. Routaboul, M. Gonidec, L. Poggini, P. Braunstein, B. Doudin, X. Xu, A. Enders, E. Zurek and P. A. Dowben, *Adv. Mater.*, 2017, **29**, 1702257.
11 B. Warner, J. C. Oberg, T. G. Gill, F. El Hallak, C. F. Hirjibehedin, M. Serri, S. Heutz, M.-A. Arrio, P. Sainctavit, M. Mannini, G. Poneti, R. Sessoli and P. Rosa, *J. Phys. Chem. Lett.*, 2013, **4**, 1546–1552.
12 X. Zhang, A. T. N'Diaye, X. Jiang, X. Zhang, Y. Yin, X. Chen, X. Hong, X. Xu and P. A. Dowben, *Chem. Commun.*, 2018, **54**, 944–947.
13 X. Zhang, S. Mu, G. Chastanet, N. Daro, T. Palamarciuc, P. Rosa, J.-F. Létard, J. Liu, G. E. Sterbinsky, D. A. Arena, C. Etrillard, B. Kundys, B. Doudin and P. A. Dowben, *J. Phys. Chem. C*, 2015, **119**, 16293–16302.
14 G. Hao, A. Mosey, X. Jiang, A. J. Yost, K. R. Sapkota, G. T. Wang, X. Zhang, J. Zhang, A. T. N'Diaye, R. Cheng, X. Xu and P. A. Dowben, *Appl. Phys. Lett.*, 2019, **114**, 032901.
15 B. Rösner, M. Milek, A. Witt, B. Gobaut, P. Torelli, R. H. Fink and M. M. Khusniyarov, *Angew. Chem.*, 2015, **127**, 13168–13172.
16 C. Etrillard, V. Faramarzi, J.-F. Dayen, J.-F. Letard and B. Doudin, *Chem. Commun.*, 2011, **47**, 9663.
17 F. Guillaume, Y. A. Tobon, S. Bonhommeau, J.-F. Létard, L. Moulet and E. Freysz, *Chemical Physics Letters*, 2014, **604**, 105–109.
18 L. Poggini, M. Gonidec, J. H. González-Estefan, G. Pecastaings, B. Gobaut and P. Rosa, *Adv. Electron. Mater.*, 2018, **4**, 1800204.
19 Y. Hasegawa, S. Kume and H. Nishihara, *Dalton Trans.*, 2009, 280–284.
20 K. Takahashi, Y. Hasegawa, R. Sakamoto, M. Nishikawa, S. Kume, E. Nishibori and H. Nishihara, *Inorg. Chem.*, 2012, **51**, 5188–5198.
21 M. Milek, F. W. Heinemann and M. M. Khusniyarov, *Inorg. Chem.*, 2013, **52**, 11585–11592.
22 T. K. Ekanayaka, H. Kurz, A. S. Dale, G. Hao, A. Mosey, E. Mishra, A. T. N'Diaye, R. Cheng, B. Weber and P. A. Dowben, *Mater. Adv.*, 2021, **2**, 760–768.
23 R. D. Schmidt, D. A. Shultz and J. D. Martin, *Inorg. Chem.*, 2010, **49**, 3162–3168.
24 R. D. Schmidt, D. A. Shultz, J. D. Martin and P. D. Boyle, *J. Am. Chem. Soc.*, 2010, **132**, 6261–6273.
25 L. Kipgen, M. Bernien, F. Nickel, H. Naggert, A. J. Britton, L. M. Arruda, E. Schierle, E. Weschke, F. Tuczek and W. Kuch, *J. Phys.: Condens. Matter*, 2017, **29**, 394003.
26 L. Kipgen, M. Bernien, S. Ossinger, F. Nickel, A. J. Britton, L. M. Arruda, H. Naggert, C. Luo, C. Lotze, H. Ryll, F. Radu, E. Schierle, E. Weschke, F. Tuczek and W. Kuch, *Nat Commun*, 2018, **9**, 2984.
27 A. Mohamed, M. Lee, K. Kitase, T. Kitazawa, J.-Y. Kim and D.-Y. Cho, *Crystals*, 2018, **8**, 433.
28 D. Collison, C. D. Garner, C. M. McGrath, J. F. W. Mosselmans, M. D. Roper, J. M. W. Seddon, E. Sinn and N. A. Young, *J. Chem. Soc., Dalton Trans.*, 1997, 4371–4376.
29 T. M. Francisco, W. J. Gee, H. J. Shepherd, M. R. Warren, D. A. Shultz, P. R. Raithby and C. B. Pinheiro, *J. Phys. Chem. Lett.*, 2017, **8**, 4774–4778.
30 M. Bernien, et al., *ACS Nano*, 2015, **9**, 8960–8966.
31 T. Miyamachi, M. Gruber, V. Davesne, M. Bowen, S. Boukari, L. Joly, F. Scheurer, G. Rogez, T. K. Yamada, P. Ohresser, E. Beaurepaire and W. Wulfhekel, *Nat Commun*, 2012, **3**, 938.
32 E. Evangelio and D. Ruiz-Molina, *Comptes Rendus Chimie*, 2008, **11**, 1137–1154.
33 M. A. Ribeiro, D. E. Stasiw, P. Pattison, P. R. Raithby, D. A. Shultz and C. B. Pinheiro, *Crystal Growth & Design*, 2016, **16**, 2385–2393.
34 L. Poggini, M. Milek, G. Londi, A. Naim, G. Poneti, L. Squillantini, A. Magnani, F. Totti, P. Rosa, M. M. Khusniyarov and M. Mannini, *Mater. Horiz.*, 2018, **5**, 506–513.
35 J.-Y. Son, K. Takubo, D. Asakura, J. W. Quilty, T. Mizokawa, A. Nakamoto and N. Kojima, *J. Phys. Soc. Jpn.*, 2007, **76**, 084703.
36 C. T. Chen, Y. U. Idzerda, H.-J. Lin, N. V. Smith, G. Meigs, E. Chaban, G. H. Ho, E. Pellegrin and F. Sette, *Phys. Rev. Lett.*, 1995, **75**, 152–155.
37 B. Weber, *Koordinationschemie: Grundlagen und aktuelle Trends*, Springer Spektrum, Berlin Heidelberg, 2014.